Supporting Information

Fleissner et al. 10.1073/pnas.1111420108

SI Materials and Methods

Expression and Purification of a Covalent T4 Lysozyme-Substrate Adduct Mutant. The T4 lysozyme 44-48RX mutant was expressed and purified according to the procedure described in Fleissner et al. (1), with the following modifications: (*i*) After induction with IPTG, mutants were incubated at 30 °C for approximately 20 h; (*ii*) following lysis by sonication, lysates were allowed to nutate at ambient temperature overnight so that the lysozyme could react with substrate; (*iii*) during cation exchange chromatography, the enzyme-substrate adduct eluted from the cation exchange column at approximately 0.1 M NaCl, whereas the unbound enzyme eluted at approximately 0.2 M; (*iv*) the enzyme-substrate adduct was further purified by gel filtration chromatography using a Superdex 75 HR 10/30 column (Amersham) as described in ref. 1. By SDS-PAGE, the substrate adduct bound enzyme was >95% pure, and its mass was noticeably different from the unbound enzyme.

Saturation Recovery (SR)–Electron-Electron Double Resonance (ELDOR). In all SR–ELDOR studies, 3–5 μL of sample were loaded into a gas-permeable TPX capillary (methylpentene polymer, i.d. = 0.6 mm, Molecular Specialties, Inc.). SR–ELDOR spectra were recorded on a Bruker E-580 spectrometer fitted with a two-loop one-gap resonator (Medical Advances) (2) and modified to use a Stanford Research Instruments amplifier (Part no. SR445A) in place of the built-in video amplifier (3). Temperature and nitrogen atmosphere around the samples were controlled by the commercial Bruker temperature control unit, which employs a flow of heated N_2 from a liquid nitrogen boiler; this equilibration was allowed to occur for 15 min prior to recording spectra to ensure no relaxation effects due to the presence of oxygen. Acquisition of data was under the control of Bruker-supplied software, and selection of short-pulse experimental parameters followed general guidelines by Hyde (4, 5). The frequency of the 1,500-mW, 100-ns pump pulse provided by the spectrometer ELDOR source was set to the rising edge of the low-field line (3 G downfield of the $\theta = 0°$ orientation; see Fig. 4*A* of the main text). The 100-μW continuous-wave(CW) detection was set to the field corresponding to the $\theta = 90°$ orientation of the nitroxide in the same manifold ($M_I = 1$), 10–15 G upfield of the pulse, or at the $\theta = 0°$ orientation in the $M_I = 0$ manifold. The defense pulse length was 280 ns, and each recovery curve was acquired with 2,048 points at 50 MHz, with an analog bandwidth of 20 MHz. Sixteen scans of 131,072 accumulations were acquired on- and off-resonance using a 1-Hz field step of −40 G (downfield). The total number of accumulations in each spectrum was thus 2.10 million over the course of approximately 6 min; each measurement was independently repeated 2–4 times.

In each case, 60 data points (out of 2,048) were trimmed from the beginning of the relaxation curves to remove remnants of the instrumental defense pulse. The spectra were then fit globally together with SR curves of spectral center lines using GraphPad Prism v5.02 data analysis software for Windows (GraphPad Software, www.graphpad.com) for three exponential recovery time constants. Each SR–ELDOR recovery curve was vertically normalized for total spin concentration and relative low-field line absorption intensity, allowing for qualitative visual comparison of all traces shown.

4-Pyridine Disulfide (4-PDS) Assay for Protein Thiol Content. The 4-PDS reagent was obtained from Sigma (sold as Aldritiol™-4). For thiol assays, fresh stock solutions of 4-PDS (100 mM in non-denatured ethanol) were prepared and used only for that day. Protein solutions were desalted using a HighPrep 26/10 (GE Healthcare) just prior to the assay. To each freshly desalted protein solution (i.e., 50 μM T4L in 50 mM MOPS, pH 6.8 or 50 μM iFABP in 50 mM sodium phosphate, 25 mM NaCl, pH 7.3), 4-PDS was added to a final concentration of 0.5 mM, and then the mixture allowed to incubate at room temperature for at least 10 min. Following incubation, the absorbance of the solution at 324 nm was measured and used to calculate the concentration of thiol present in solution [ε_{324} of 4-thiopyridone = 19,800 $M^{-1}\,cm^{-1}$ (6)]. Positive controls (cysteine mutants of either T4L or iFABP) were assayed each day to verify expected thiol content (Table S1).

Effective Hamiltonian Simulations for T4L 5-9RX on Sepharose. The spectrum of T4L 5-9RX on Sepharose has a classic "powder" lineshape; i.e., that of an ensemble of completely immobilized nitroxides at random orientations. The $2A_{zz}'$ is 70.7 G, compared to the average value of 74.9 G in frozen solution where all motion is absent. The difference is due to the internal modes in the RX side chain, with possible contributions from motion in the protein backbone. The macroscopic order with microscopic disorder (MOMD) fit (7) shown in Fig. 1 of the main text is consistent with a fast internal motion and high order. If this is the case, the spectrum should be approximately accounted for by a time-independent effective Hamiltonian (8, 9). In this model, the motion is assumed to be sufficiently rapid to average the magnetic parameters of the nitroxide over the space of the restricted motion. Taking $2A_{zz}' = 70.7$ G and assuming an axially symmetric motion in a cone, the averaged values of the magnetic parameters consistent with this value of $2A_{zz}'$ can be readily computed (10) from the average principal values in the absence of motion given in Table S2. The results are: $A_{xx}' = A_{yy}' = 6.0$; $A_{zz}' = 35.4$; $g_{xx}' = g_{yy}' = 2.00746$; $g_{zz}' = 2.00262$. Simulation of a powder spectrum using these values gives the red trace in Fig. S3*A*; the reasonably good agreement with the experimental spectrum (black trace, Fig. S3*A*) supports the fast motion–high order model for RX. The order parameter corresponding to the averaged parameters is $S = 0.87$.

The effective Hamiltonian model may be used to simulate the spectra in the presence of rotational diffusion of the protein. For this purpose, the effective Hamiltonian magnetic parameters given above are used as input parameters in a least-squares fit to the experimental spectra using the MOMD fitting program (7) as implemented by Christian Altenbach (http://sites.google.com/site/altenbach/). In the fit, the only dynamic parameter varied is the isotropic rotational correlation time of the protein. The red traces in Fig. S3 *B* and *C* are fits to T4L 5-9RX in 30% sucrose and buffer respectively; the black traces are the experimental spectra. The corresponding correlation times from the fits are 35 and 9 ns, respectively. These values are in good agreement with those obtained with global multifrequency fits to spin-labeled T4L using the SRLS model (11).

Sensitivity of a Nitroxide Spin Label to Fast (Nanosecond) Backbone Motions. For a nitroxide undergoing rapid but constrained fluctuations, the value of A_{zz}' is an approximate measure of the amplitude. For this situation, one measure of spectral sensitivity to changes in the fluctuation angle (θ) is the first derivative of A_{zz}' with respect to angle ($dA_{zz}'/d\theta$), which depends on the absolute value of θ, as shown in Fig. S6.

For an essentially rigid side chain with $\theta \approx 0$, the sensitivity for detecting small differences in θ from site-to-site in a protein due, for example, to contributions from backbone fluctuations, is very low ($dA_{zz}'/d\theta$ is near zero). On the other hand, the internal modes in a flexible side bias the nitroxide motion into a region of larger θ where the sensitivity to small changes in θ is high. For example, the internal motion of the common R1 side chain results in fluctuations of the nitroxide with apparent amplitude of about 36° (8); this is close to the angle where A_{zz}' is maximally sensitive to changes in θ. Thus, R1 is a good choice of side chain to detect small differences in nanosecond backbone motion. For RX, which has apparent amplitude of approximately 15° because of internal motion, the sensitivity is about a factor of two lower.

1. Fleissner MR, Cascio D, Hubbell WL (2009) Structural origin of weakly ordered nitroxide motion in spin-labeled proteins. *Protein Sci* 18: 893–908.
2. Hubbell WL, Froncisz W, Hyde JS (1987) Continuous and stopped flow electron-paramagnetic-resonance spectrometer based on a loop gap resonator. *Rev Sci Instrum* 58:1879–1886.
3. Bridges MD, Hideg K, Hubbell WL (2010) Resolving conformational and rotameric exchange in spin-labeled proteins using saturation recovery EPR. *Appl Magn Reson* 37: 363–390.
4. Percival PW, Hyde JS (1976) Saturation-recovery measurements of spin-lattice relaxation-times of some nitroxides in solution. *J Magn Reson* 23:249–257.
5. Hyde JS (1979) Saturation recovery methodology. *Time Domain Electron Spin Resonance*, eds Kevan L, Schwartz RN (Wiley, New York), pp 1–30.
6. Grassetti DR, Murray JF, Jr. (1967) Determination of sulfhydryl groups with 2,2′- or 4,4′-dithiodipyridine. *Arch Biochem Biophys* 119:41–49.
7. Budil DE, Lee S, Saxena S., Freed JH (1996) Nonlinear-least-squares analysis of slow-motion EPR spectra in one and two dimensions using a modified Levenberg–Marquardt algorithm. *J Magn Reson A* 120:155–189.
8. Hubbell WL, McConnell HM (1971) Molecular motion in spin-labeled phospholipids and membranes. *J Am Chem Soc* 93:314–326.
9. Columbus L, Kálai T, Jeko J, Hideg K, Hubbell WL (2001) Molecular motion of spin labeled side chains in alpha-helices: Analysis by variation of side chain structure. *Biochemistry* 40:3828–3846.
10. Griffith OH, Jost PC (1976) Lipid spin labels in biological membranes. *Spin Labeling Theory and Applications*, ed Berliner LJ (Academic, New York) pp 454–523.
11. Zhang Z, et al. (2010) Multifrequency electron spin resonance study of the dynamics of spin labeled T4 lysozyme. *J Phys Chem B* 114:5503–5521.

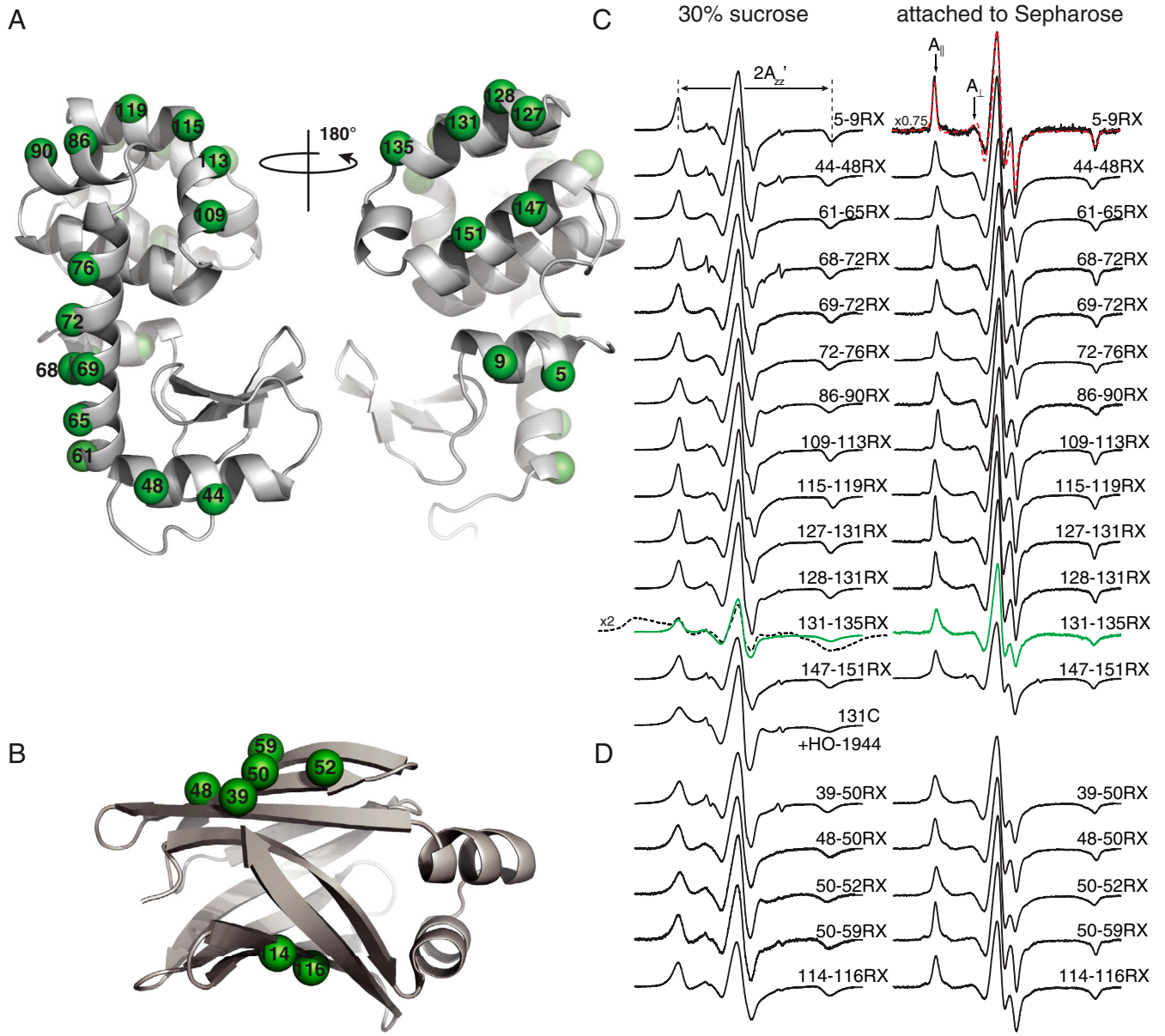

Fig. S1. Sites for introduction of the RX side chain into T4 Lysozyme (T4L) and intestinal fatty acid-binding protein (iFABP), and the corresponding EPR spectra. (*A* and *B*) Ribbon models of wild-type T4L [*A*, PDB ID code 1L63 (1)] and iFABP (*B*, PDB ID code 2IFB (2)] highlighting the solvent-exposed sites used in this study with spheres at their α-carbons; (*C* and *D*) Area-normalized, room temperature EPR spectra of the complete set of T4L (*C*) and iFABP (*D*) RX mutants in either a 30% (wt/vol) sucrose solution (*Left*) or attached to CNBr-activated Sepharose in buffer (*Right*). Overlaid on the Sepharose-bound spectrum for T4L 5–9RX is nonlinear least-squares fit to an MOMD model (red-dashed trace). The dashed spectrum for T4L 131–135RX in 30% sucrose was obtained after reaction with a 10:1 HO-1944:protein ratio; the scan width was increased to 125 G and the vertical intensity doubled to reveal the significant broadening from spin–spin interactions. When labeled with a 1:1 ratio, the broadening was reduced (green traces, in 30% sucrose and Sepharose-attached).

1 Nicholson H, Anderson DE, Dao Pin S, Matthews BW (1991) Analysis of the interaction between charged side chains and the alpha-helix dipole using designed thermostable mutants of phage T4 lysozyme. *Biochemistry* 30:9816–9828.

2 Sacchettini JC, Gordon JI, Banaszak LJ (1989) Crystal structure of rat intestinal fatty-acid-binding protein. Refinement and analysis of the *Escherichia coli*-derived protein with bound palmitate. *J Mol Biol* 208:327–339.

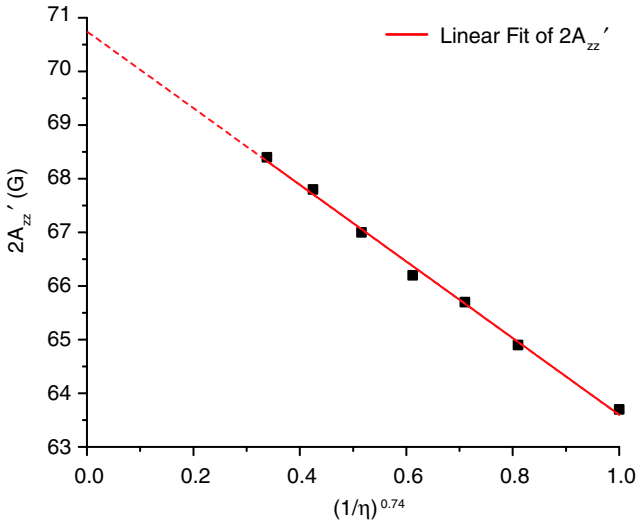

Fig. S2. The viscosity dependence of $2A_{zz}'$ for T4L 5-9RX in sucrose solution at constant temperature. Approximately 100 μM protein was prepared in sucrose concentrations ranging from 0 to 35% wt/wt in buffer (50 mM MOPS, 25 mM NaCl pH 6.8). Viscosities of the sucrose solutions were taken from CRC handbook (1). At each concentration, $2A_{zz}'$ was determined at 295 K and plotted vs. the function of viscosity as indicated. Linear extrapolation of the plot to infinite viscosity yields $2A_{zz}'$ in the limit of zero rotational diffusion of the protein (70.8 G for this mutant). The principle of this analysis is that variation of bulk viscosity has little influence on internal motion of side chains, but results in a Stokes–Einstein-like modulation of protein rotational diffusion; this has been demonstrated for R1 in proteins (2).

1 *CRC Handbook of Chemistry and Physics*, ed Lide DR (CRC Press, Boca Raton, FL), 61st Ed, pp D240 and D270.
2 Timofeev VP, Tsetlin VI (1983) Analysis of mobility of protein side-chains by spin label technique. *Biophys Struct Mech* 10:93–108.

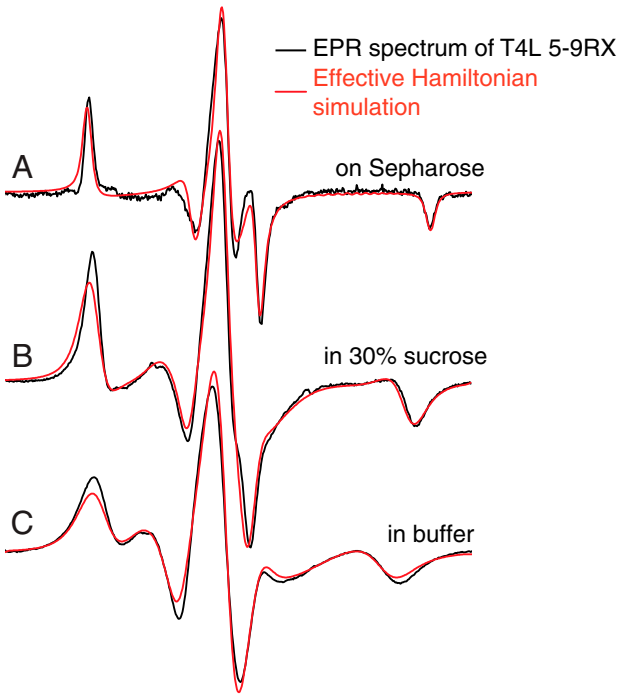

Fig. S3. A comparison of the CW EPR data (black traces) to time-independent effective Hamiltonian simulations (red traces) for T4L 5-9RX. (*A*) Attached to Sepharose. (*B*) In 30% sucrose in buffer. (*C*) In buffer. All spectra were recorded at 295 K with 100-G scan width; the buffer used was 50 mM MOPS, 25 mM NaCl, pH 6.8.

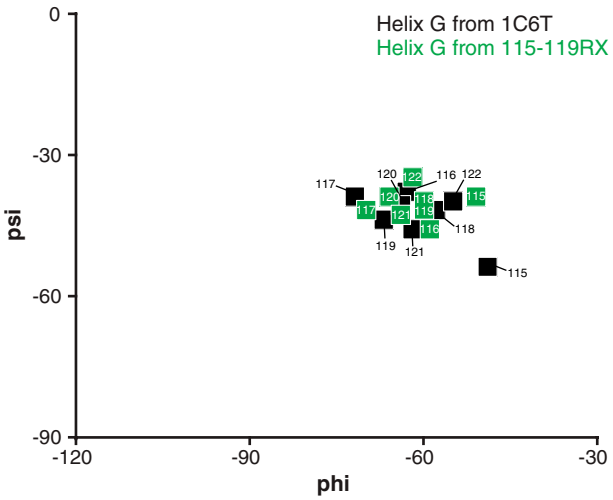

Fig. S4. Ramachandran plot of the backbone dihedral angles for the T4L wild type and 115-119RX crystal structures, showing that RX does not substantially perturb the local protein structure from the wild type.

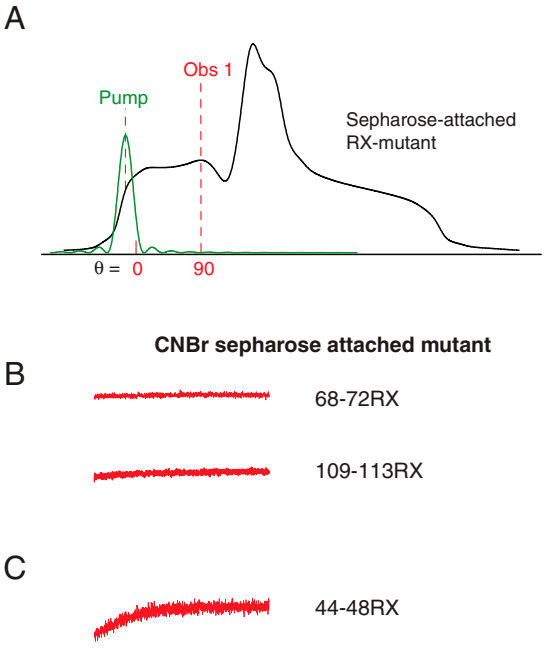

Fig. S5. ELDOR studies of sepharose-attached RX-crosslinked T4L mutants not shown in Fig. 4. (*A*) A representative EPR absorption spectrum, again showing the fields at which the saturating pulse was applied (Pump) and at which the arrival and recovery of saturation was observed (Obs 1: Intramanifold spectra). (*B*) Intramanifold curves for 68-72RX (*Upper*) and 109-113RX (*Lower*) indicating no transfer of saturation by rotational diffusion. (*C*) Intramanifold curve for the T4L 44-48RX mutant at 298 K. The recovery curves in *B* and *C* are 40 μs wide.

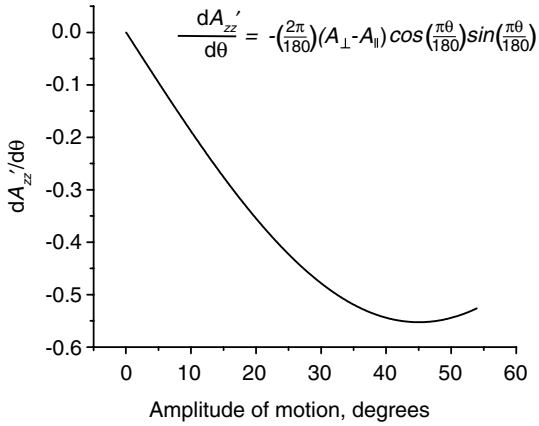

Fig. S6. Sensitivity of A_{zz}' to changes in amplitude of fast motion within a cone. The amplitude is measured as the half-angle of the cone; $A_{\perp}$ and $A_{||}$ are the principal values of the axial hyperfine tensor.

Table S1. Results of a 4,4′-dithiodipyridine (4-PDS) assay of T4L and rIFABP RX mutants for the determination of free (unreacted) thiol groups on proteins

Mutant	Protein, μM	$A_{324\,nm}$	% free thiol in solution*
T4L mutants			
5-9RX	50	0.0039	0.20%
44-48RX	50	−0.0009	−0.05%
61-65RX	50	0.0060	0.30%
68-72RX	50	0.0335	1.69%
69-72RX	50	0.0300	1.52%
72-76RX	50	0.0054	0.27%
86-90RX	50	0.0296	1.49%
109-113RX	50	0.0078	0.39%
115-119RX	50	0.0028	0.14%
128-131RX	50	0.0066	0.33%
127-131RX	50	0.0071	0.36%
131-135RX	50	0.0265	1.34%
147-151RX	50	0.0098	0.49%
61C/65C	29	1.1400	99.27%
86C/90C	38	1.4944	99.31%
131C/151C	10.5	0.4214	101.35%
rIFABP mutants			
39-50RX	50	0.0332	1.68%
48-50RX	50	0.0008	0.04%
50-52RX	50	0.0026	0.13%
50-59RX	50	−0.0044	−0.22%
114-116RX	50	−0.0061	−0.31%
116-118RX	50	0.0106	0.54%
48C/50C	50	1.9795	99.97%
50C/52C	50	2.0411	103.09%

*Percent free thiol was computed according to the procedure described in *SI Materials and Methods*.

Table S2. Principal magnetic tensor, $2A_{zz}'$, and *S* values for RX mutants attached to Sepharose in buffer and $2A_{zz}'$ values for the mutants in a 30% sucrose solution

	Principal magnetic tensor values* †								
Mutant	A_{xx}	A_{yy}	A_{zz}	g_{xx}	g_{yy}	g_{zz}	$2A_{zz}'$, 30% sucrose	$2A_{zz}'$, Sepharose	*S*, Sepharose‡
T4L mutants									
5–9RX							67.5	70.7	0.90
44–48RX	5.85	3.92	37.60	2.0079	2.0063	2.0018	65.5	69.1	0.86
61–65RX	5.84	4.11	37.65	2.0087	2.0063	2.0023	66.8	69.7	0.87
68–72RX	5.95	4.04	37.20	2.0086	2.0067	2.0023	66.5	69.7	0.89
69–72RX	5.97	3.99	37.52	2.0087	2.0067	2.0023	67.3	70.4	0.89
72–76RX	5.86	4.09	37.35	2.0087	2.0068	2.0023	66.3	70.0	0.89
86–90RX	5.91	4.08	37.62	2.0086	2.0068	2.0023	65.8	69.6	0.87
109–113RX	5.91	4.28	37.29	2.0087	2.0067	2.0023	66.4	69.3	0.88
115–119RX	6.05	3.86	37.12	2.0087	2.0068	2.0023	68.1	70.5	0.91
127–131RX	5.87	4.01	37.33	2.0087	2.0068	2.0023	67.3	69.7	0.89
131–135RX	5.95	5.95	37.57	2.0086	2.0067	2.0023	67.2	69.3	0.87
147–151RX	5.96	4.04	37.25	2.0087	2.0068	2.0023	66.3	69.6	0.89
iFABP mutants									
39–50RX	5.65	4.06	37.76	2.0087	2.0068	2.0023	66.6	70.4	0.88
48–50RX	5.91	4.06	37.50	2.0086	2.0067	2.0023	66.8	70.8	0.90
50–52RX	5.86	3.98	37.64	2.0087	2.0067	2.0023	64.8	69.6	0.87
50–59RX	6.01	3.80	37.67	2.0087	2.0067	2.0023	66.3	70.5	0.89
114–116RX	6.23	3.96	37.28	2.0087	2.0067	2.0023	63.7	70.3	0.90
Average	5.93	4.01	37.47	2.0086	2.0067	2.0023	66.6	70.0	0.89
Standard deviation	0.11	0.11	0.19	0.0002	0.0001	0.0001	1.1	0.6	0.01

*Principal *A* and *g* tensor values were determined from CW spectra of proteins on Sepharose frozen at −50 °C; $2A_{zz}'$ values were measured directly from the spectrum.

†A_{xx}, A_{yy}, A_{zz}, and $2A_{zz}'$ are in units of Gauss.

‡*S* was computed according to $S = 3(A_{zz}' - A_o)/(2A_{zz} - (A_{xx} + A_{yy}))$, where $A_o = 1/3(A_{xx} + A_{yy} + A_{zz})$ and A_{zz}' is taken directly from the large hyperfine splitting ($2A_{zz}'$) for the corresponding mutant. For T4L 5-9RX, *S* was computed using average principal *A* and *g* tensor values for all mutants measured.

Table S3. X-ray data collection and refinement statistics for the T4L 115-119RX crystal

Data collection	
Reflections observed	175,628
Unique reflections	18,829
Temperature, K	100
Wavelength, Å	1.5418
Resolution, Å	80–1.80
Highest resolution shell	1.86–1.80
Space group	$P3_221$
R_{sym}, %	7.2 (44.2)
I/σ	12.3 (5.5)
Completeness, %	97.4 (80.9)
Unit cell dimensions	
a, Å	60.113
b, Å	60.113
c, Å	96.655
Refinement	
Resolution, Å	35.42–1.80
Reflections used	18,802
R_{cryst}, %	18.7
R_{free}, %	23.2
Number of non-H atoms	
protein	1,318
nonprotein	189
Rms deviations	
Bond lengths, Å	0.006
Bond angles, °	1.116
Average B factor, Å^2	
protein atoms	20.3
nonprotein atoms	27.3
Estimated coordinate error, Å	0.21
Protein Data Bank ID code	3L2X